ACS APPLIED MATERIALS & INTERFACES

Research Article

www.acsami.org

Synthesis, Structure, and Ethanol Gas Sensing Properties of In_2O_3 Nanorods Decorated with Bi_2O_3 Nanoparticles

Sunghoon Park, Soohyun Kim, Gun-Joo Sun, and Chongmu Lee*

Department of Materials Science and Engineering, Inha University, Yonghyun-dong, Nam-gu, Incheon 402−751, Republic of Korea

Supporting Information

ABSTRACT: Bi_2O_3-decorated In_2O_3 nanorods were synthesized using a one-step process, and their structure, as well as the effects of decoration of In_2O_3 nanorods with Bi_2O_3 on the ethanol gas-sensing properties were examined. The multiple networked Bi_2O_3-decorated In_2O_3 nanorod sensor showed responses of 171−1774% at ethanol concentrations of 10−200 ppm at 200 °C. The responses of the Bi_2O_3-decorated In_2O_3 nanorod sensor were stronger than those of the pristine-In_2O_3 nanorod sensors by 1.5−4.9 times at the corresponding concentrations. The two sensors exhibited short response times and long recovery times. The optimal Bi concentration in the Bi_2O_3-decorated In_2O_3 nanorod sensor and the optimal operation temperature of the sensor were 20% and 200 °C, respectively. The Bi_2O_3-decorated In_2O_3 nanorod sensor showed selectivity for ethanol gas over other gases. The origin of the enhanced response, sensing speed, and selectivity for ethanol gas of the Bi_2O_3-decorated In_2O_3 nanorod sensor to ethanol gas is discussed.

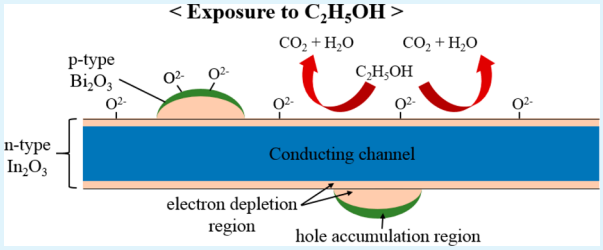

KEYWORDS: *In_2O_3, Bi_2O_3, nanorods, gas sensor, ethanol*

1. INTRODUCTION

Metal oxide semiconductors (MOS) have several advantages as sensor materials, such as high sensitivity, fast response and recovery, low detection limits, low fabrication cost, simplicity in fabrication, measurement, and function durability compared to other semiconductors.[1,2] On the other hand, the high operation temperature is a disadvantage of metal oxide semiconductor-based sensors. One technique to solve this problem is to use one-dimensional (1D) nanostructured sensors with high surface-to-volume ratios[3−5] because of the larger change in electrical resistance because of more significant gas adsorption in 1D nanostructures. Another is to dope or decorate the metal oxide with metal or metal oxide nanoparticles. Noble metals and transition metals, such as Pd, Pt, Au, Ag, Cu, and Cr are commonly adopted as catalyst metals.[6−8] A third procedure is to form heterostructures by coating one type of metal oxide nanostructures with another type of metal oxide thin film, that is, forming a core−shell structure[9−13] or decorating one type of metal oxide nanostructure with another type metal oxide nanoparticles.[14−22] As listed in Table 1 a range of metal oxides have been used for the latter purposes, but there have been no reports of the use of Bi_2O_3 in decorating MOS sensors.[14−22] Only the enhanced photoluminescence of Bi_2O_3-decorted ZnO nanorods and the enhanced photocatalysis of Bi_2O_3-decorted TiO_2 nanotubes were found in the literature.[23,24]

Of the above-mentioned metal oxide semiconductors, In_2O_3, has been reported to have high sensitivities to many gases, such as H_2, CO, NO_2, NH_3, O_3, and Cl_2.[25−28] In particular, In_2O_3-based sensors have been reported to be highly selective to ethanol gas.[29] Pt and La_2O_3-loaded hot-wire type ultrafine In_2O_3 sensors were found to be highly selective to ethanol gas.[15] Thin film-type In_2O_3 sensors have limited sensitivity because of relatively low surface-to-volume ratios. Most In_2O_3 thin film devices are commonly operated at high temperatures (200−600 °C) to enhance their chemical reactivity, but high operating temperature is a drawback for practical applications. On the other hand, one-dimensional (1D) nanostructures with various morphologies such as nanorods, nanowires, nanofibers, nanoneedles, and nanopushpins were used for the sensing tests. Of those sensing test results, Table 2 lists the previous results obtained using In_2O_3 1D nanostructures. In_2O_3 nanowires, In_2O_3 nanorods, and In_2O_3 nanofibers were showed responses of 25.3, 11.5, and 379 to 1000, 50, and 15 000 ppm of C_2H_5OH at 370, 300, and 300 °C, respectively.[30,31]

A range of methods, such as chemical vapor deposition, evaporation, electrospinning, sol−gel, carbothermal reduction, and solvothermal techniques have been employed for the synthesis of In_2O_3 1D nanostructures.[32] Pt nanoparticles were deposited on electrospun In_2O_3 nanofibers by adding H_2PtCl_6 aqueous solution into the water containing the as-prepared nanofibers and heated to boiling.[33] *P*-aminophenyl trimethoxysilane was used to functionalize the Au nanoparticles on the surface of the nanowires grown by CVD.[34] Similarly, CVD-grown In_2O_3 nanowires were functionalized with Pt nanoparticles by sputter-deposition of Pt, followed by annealing at 800 °C for 30 min in Ar ambient.[35] On the other hand, one-step process for the preparation of In_2O_3 1D nanostructures

Received: February 2, 2015
Accepted: April 6, 2015
Published: April 6, 2015

DOI: 10.1021/acsami.5b00972
ACS Appl. Mater. Interfaces 2015, 7, 8138−8146

Table 1. List of Decoration Materials in 1D Nanostructured Metal Oxide Semiconductor Sensors Decorated with Other Metal Oxide Semiconductor Nanoparticles along with Their Sensing Properties

decoration material	1D nanomaterial	target gas	results	ref
CuO	SnO_2	H_2S	improved sensitivity and selectivity for H_2S	14
Bi_2O_3	TiO_2 NT		.	
La_2O_3	In_2O_3	C_2H_5OH	prominent selectivity for C_2H_5OH	15
NiO	ZnO	C_2H_5OH	design of highly sensitive volatile organic compound sensors by controlling NiO loading on ZnO nanowire networks	16
In_2O_3	NiO	C_2H_5OH	enhanced ethanol sensing with In_2O_3-decorated NiO hollow nanostructures via modulation of hole accumulation layers	17
ZnO	SnO_2	H_2S	enhanced photon- and gas-sensing properties of a single SnO_2 nanowire sensor functionalized with nanoparticles	18
NiO		CO, CH_4		
TiO_2	GaN	cyclohexane, benzene, chlorobenzene, toluene, ethylbenzene, xylene	highly selective GaN-nanowire TiO_2-nanocluster hybrid sensors for detection of benzene and related environment pollutants	19
Cr_2O_3	n-SnO_2	reducing gases (benzene, toluene, CO, H_2)	prominent reducing gas-sensing performances of n-SnO_2 nanowires by local creation of p−n heterojunctions and functionalization with p-Cr_2O_3 nanoparticles	20
Co_3O_4	ZnO	NO_2, C_2H_5OH	selective detection of NO_2 and C_2H_5OH using a Co_3O_4-decorated ZnO nanowire network sensor	21
Fe_2O_3	V_2O_5	C_2H_5OH	synthesis and gas sensing properties of Fe_2O_3 nanoparticles activated V_2O_5 nanotubes	22

Table 2. Comparison of the Responses of In_2O_3 1D Nanostructures to C_2H_5OH Gas[a]

nanostructures	T (°C)	concentration (ppm)	response (%)	ref
In_2O_3 NRs	200	200	360	present work
Bi_2O_3 nanoparticle-decorated In_2O_3 NRs	200	200	1774	present work
In_2O_3 NRs	370	1000	25 300	30
In_2O_3 NRs	370	50	11 500	30
In_2O_3 NFs	300	15 000	37 900	31

[a]NR and NF denote nanorod and nanofiber, respectively. NRs denotes nanorods.

functionalized with metal or metal oxide nanoparticles have not been reported before to the best of the authors' knowledge.

Several studies have examined Bi_2O_3-other metal oxide heterostructured sensors. The effects of Bi_2O_3 content on the H_2 gas sensing properties of ZnO varistor gas sensor have been examined.[36] WO_3−Bi_2O_3 mixed screen-printed thick films with a range of Bi_2O_3 contents (3−50 wt %) have been studied as a promising sensitive material for NO gas sensors.[37] The gas-sensitivity of the WO_3−Bi_2O_3 mixed thick films are strongly dependent on the Bi_2O_3 content.[38] SnO_2−Bi_2O_3 nanoparticle gas sensors are sensitive to O_2 and CO gases.[39] The enhanced gas sensing performance of Bi_2O_3-core/In_2O_3-shell nanorod gas sensors has been reported.[40] Bi_2O_3 nanowire sensors have been reported to be highly sensitive to part per million levels of NO_2 in ambient air with fast response, good selectivity, and stability.[41] On the other hand, there are no reports of Bi_2O_3 nanoparticle-decorated In_2O_3 nanorods. In this study, Bi_2O_3 nanoparticle-decorated In_2O_3 nanorods were synthesized using a one-step process, and their structure and ethanol gas sensing performance of multiple-networked In_2O_3 nanorod sensors decorated with Bi_2O_3 nanoparticles were examined.

2. EXPERIMENTAL SECTION

Bi_2O_3 nanoparticle-decorated In_2O_3 nanorods were prepared using a single-step process. First, Si (100) substrates were used for the synthesis of one-dimensional (1D) In_2O_3 nanostructures. A 3 nm-thick Au thin film was deposited on Si substrates by direct current (dc) magnetron sputtering. A quartz tube was mounted horizontally inside the tube furnace. A mixture of 0.1 g Bi and 0.9 g In_2S_3 powders was placed on the lower holder at the center of the quartz tube. A Au-coated Si substrate was placed face down on the upper holder, approximately 5 mm away from the powder mixture. The furnace was heated to 800 °C at a heating rate of 10 °C/min and maintained at that temperature for 1 h in a N_2/O_2 atmosphere with constant N_2 and O_2 flow rates of 98 and 2 cm^3/min, respectively. The total pressure was set to 1.0 Torr. Subsequently, the furnace was furnace-cooled to room temperature at 1 mTorr after which the products were taken out.

The morphology and structure of the collected nanorod samples were examined by scanning electron microscopy (SEM, Hitachi S-4200,10 kV) and transmission electron microscopy (TEM, JEOL 2100F, 300 kV). Low-magnification TEM images, high-resolution TEM (HRTEM) images, and corresponding selected area electron diffraction (SAED) patterns were obtained. Energy-dispersive X-ray spectroscopy (EDXS) elemental maps were obtained using the EDXS system attached to the TEM to observe the elemental distribution in the nanorod samples. Glancing angle X-ray diffraction (XRD, Philips X'pert MRD) was carried out using Cu K_α radiation (λ = 0.1541 nm) to examine the crystal structure of the nanorod samples.

The as-synthesized pristine and Bi_2O_3 nanoparticle-decorated In_2O_3 nanorods (50 mg) were dispersed ultrasonically in ethanol. Suspensions of nanorods in ethanol were spread overoxidized Si substrates with interdigitated Pt electrodes as described elsewhere.[42] The flow-through technique was used to measure the gas sensing properties in a tube furnace with a resistance heater. The pristine or Bi_2O_3 nanoparticle-decorated In_2O_3 nanorods were inserted in the chamber. Ethanol gas diluted with dry synthetic air was injected into the quartz tube at a flow rate of 200 cm^3/min at room temperature. The electrical measurements were taken at 200 °C under 40% RH by a voltamperometric method. The electrical resistance of gas sensors was determined by measuring the electric current using a Keithley source meter-2612 with a source voltage of 1 V.

3. RESULTS AND DISCUSSION

3.1. Structure of the Bi_2O_3 Nanoparticle-Decorated In_2O_3 Nanorods. Figure 1a presents an SEM image of the Bi_2O_3 nanoparticle-decorated In_2O_3 nanorods synthesized in this study, and Figure 1b shows an enlarged SEM image of a typical In_2O_3 nanorod decorated with Bi_2O_3 nanoparticles. The diameter ranges of the nanorods and nanoparticles were 30−100 and 20−50 nm, respectively. Figure 1c shows the XRD patterns of the pristine In_2O_3 nanorods and Bi_2O_3 nanoparticle-decorated In_2O_3 nanorods. XRD showed that the Bi_2O_3 nanoparticle-decorated In_2O_3 nanorods were a combination of crystalline In_2O_3 and Bi_2O_3. The smaller reflection peaks for Bi_2O_3 than those for In_2O_3 might be due to the smaller volume

DOI: 10.1021/acsami.5b00972
ACS Appl. Mater. Interfaces 2015, 7, 8138−8146

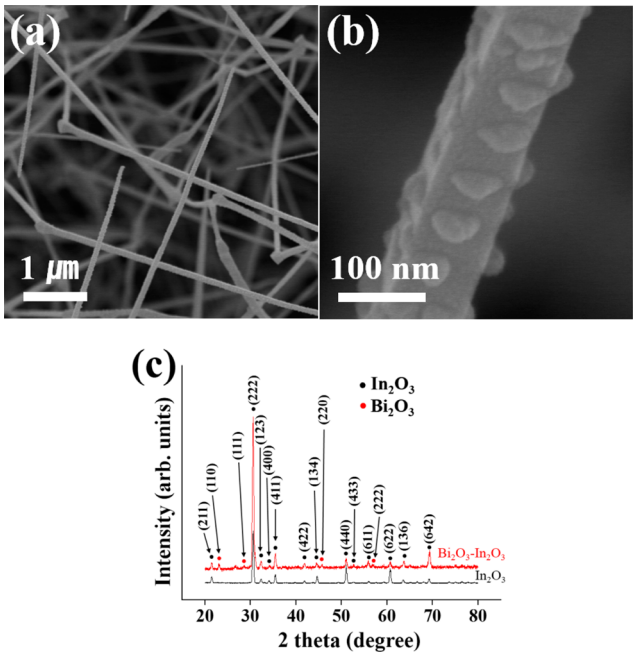

Figure 1. (a) SEM image of Bi_2O_3 nanoparticle-decorated In_2O_3 nanorods. (b) Enlarged SEM image of a typical Bi_2O_3 nanoparticle-decorated In_2O_3 nanorod. (c) XRD patterns of pristine In_2O_3 nanorods and Bi_2O_3 nanoparticle-decorated In_2O_3 nanorods.

of Bi_2O_3 nanoparticles than those of the In_2O_3 nanorods. A low-magnification TEM image (Figure 2a) exhibits a straight morphology of the pristine In_2O_3 nanorod. The fringe pattern in a high-magnification TEM image (Figure 2b) and the clear diffraction spots in the corresponding selected area electron diffraction (SAED) pattern (Figure 2c) suggests that the In_2O_3 nanorod is a single crystal. On the other hand, the low-magnification TEM image (Figure 2d) shows that the In_2O_3 nanorod is surrounded by the Bi_2O_3 nanoparticles with a ring-like morphology. On the other hand, the ring-like morphology of the Bi_2O_3 nanoparticles is not typical considering the enlarged SEM image in Figure 1b. A high-resolution TEM image (Figure 2e) showed that both In_2O_3 nanorods and Bi_2O_3 nanoparticles were single crystals as illustrated by the fringes over the entire areas of the nanorod and a nanoparticle on the nanorod. The spacings between the two neighboring parallel fringes in the darker region were 0.292 and 0.239 nm, which were assigned to the interplanar spacings of the (222) and (411) planes, respectively, of body-centered cubic-structured In_2O_3. In contrast, the spacing of the fringes in the brighter region were 0.315 and 0.385 nm, which were assigned to the interplanar spacings of the (111) and (110) planes of simple cubic-structured Bi_2O_3, respectively. The corresponding selected area electron diffraction (SAED) pattern (Figure 2f) confirmed that both In_2O_3 nanorods and Bi_2O_3 nanoparticles were single crystals by showing two different sets of spotty patterns: bcc-structured In_2O_3 and simple cubic-structured Bi_2O_3. TEM microscopy revealed no big difference in the microstructure of In_2O_3 nanorods between the pristine In_2O_3 nanorods and Bi_2O_3 nanoparticle-decorated In_2O_3 nanorods. Figure 3a–d shows the EDXS elemental maps of a typical In_2O_3 nanorod decorated with Bi_2O_3 nanoparticles. The indium map matches well with the nanorod in the TEM image and bismuth and oxygen maps matches well with the nanoparticles surrounding the nanorod in the TEM image, confirming that it is a Bi_2O_3 nanoparticle-decorated In_2O_3 nanorod.

3.2. Sensing Performance of the Pristine and Bi_2O_3 Nanoparticle-decorated In_2O_3 Nanorod Gas Sensors.

Figure 4a and b presents the electrical resistances of pristine and Bi_2O_3 nanoparticle-decorated In_2O_3 nanorod gas sensors, respectively, exposed to different ethanol concentrations. The resistance decreased to a minimum resistance immediately after exposure to ethanol and recovered completely to the initial value after stopping supply of ethanol gas. The resistance showed good reversibility during the introduction and exhaust cycles of ethanol gas. Both sensors responded to ethanol gas instantaneously and recovered slowly. The origin of the faster response than recovery is not clear, but the authors surmise it is due to the higher solid solubility of ethanol in In_2O_3 and Bi_2O_3

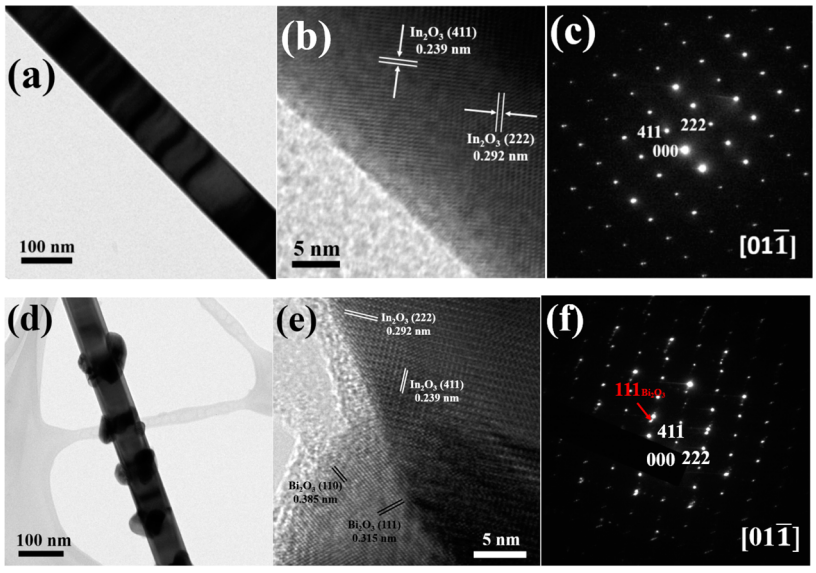

Figure 2. (a) Low-magnification TEM image, (b) high-resolution TEM image, and (c) selected area electron diffraction pattern of pristine In_2O_3 nanorods. (d) Low-magnification TEM image, (e) high-resolution TEM image, and (f) selected area electron diffraction pattern of Bi_2O_3 nanoparticle-decorated In_2O_3 nanorods.

DOI: 10.1021/acsami.5b00972
ACS Appl. Mater. Interfaces 2015, 7, 8138–8146

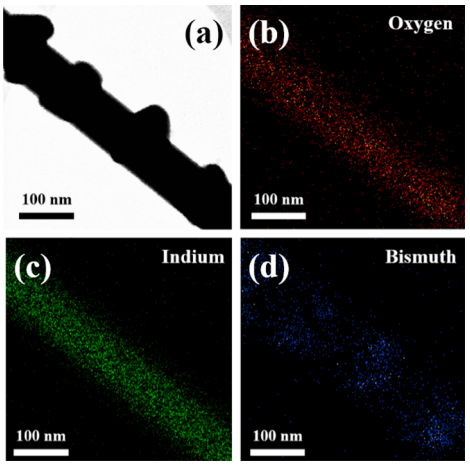

Figure 3. (a) TEM image and EDXS maps of a typical Bi_2O_3 nanoparticle-decorated In_2O_3 nanorod: (b) oxygen, (c) indium, and (d) bismuth.

than oxygen, even though the solid solubility data are not available. Figure 4c shows the responses of the two sensors to ethanol gas. The responses of both samples to ethanol gas tended to become stronger with increasing ethanol gas concentration, but the Bi_2O_3 nanoparticle-decorated In_2O_3 nanorod sensor showed a higher increasing rate. The Bi_2O_3 nanoparticle-decorated In_2O_3 nanorod sensor exhibited much stronger response than the pristine In_2O_3 nanorod sensor. The response to 200 ppm ethanol was increased almost 5-fold by the decoration of In_2O_3 nanorod with Bi_2O_3 nanoparticles. The response was defined as $[R_a/R_g]$*100% for ethanol gas, where R_a and R_g are the electrical resistances of sensors in air and ethanol gas, respectively. Table 2 compares the response of the pristine In_2O_3 nanorods and the Bi_2O_3 nanoparticle-decorated In_2O_3 nanorods synthesized by a single-step process in this study with those of the In_2O_3 nanorods measured in previous studies. The response of the pristine In_2O_3 nanorods measured in this study is somewhat weaker than those measured in previous studies,[30,31] probably because of the lower ethanol concentration and lower operation temperature. On the other hand, the response of the pristine In_2O_3 nanorods and the Bi_2O_3 nanoparticle-decorated In_2O_3 nanorods measured in this study is comparable to the previous studies despite the lower ethanol concentration and lower operation temperature.

The response and recovery times were defined as the times to reach 90% variation in resistance upon exposure to ethanol and air, respectively. The Bi_2O_3 nanoparticle-decorated In_2O_3 nanorod sensor exhibited longer response time (Figure 5a) but shorter recovery time (Figure 5b) than the pristine In_2O_3 nanorod sensor at the same ethanol concentration. The total sensing time of the former was far shorter than that of the latter because the recovery time was far longer than the response time toward ethanol gas for both sensors, which is in good agreement with previous reports.[43] Upon exposure to 200 ppm ethanol and air, the response and recovery times of the Bi_2O_3 nanoparticle-decorated In_2O_3 nanorod sensor were 24 and 180 s, respectively. In contrast, the response and recovery times of the pristine In_2O_3 nanorod sensor were 13 and 350 s, respectively. 1D nanostructures commonly show faster response and recovery than thin films.[44] It is not fully understood at present why the response time was increased by adding Bi_2O_3 nanoparticles. The authors surmise that it is due to the higher solid solubility or higher diffusivity of ethanol

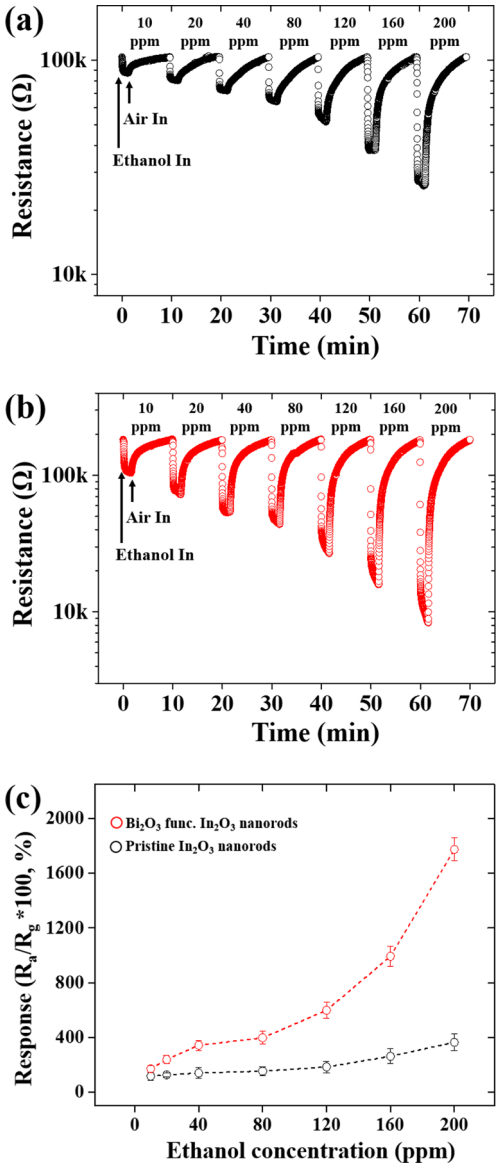

Figure 4. Dynamic responses of the (a) pristine and (b) Bi_2O_3 nanoparticle-decorated In_2O_3 nanorod gas sensors. (c) Responses of the pristine and Bi_2O_3 nanoparticle-decorated In_2O_3 nanorod gas sensors as a function of the ethanol concentration.

in In_2O_3 than in Bi_2O_3, even though the solid solubility data are not available. Bi_2O_3 decoration is thought to have lowered the solid solubility or diffusivity of ethanol in the sensor.

The responses of the Bi_2O_3 nanoparticle-decorated In_2O_3 nanorod sensors to 200 ppm of ethanol gas at 200 °C were examined to determine the optimal Bi concentration in the nanorod. Figure 6a shows strong dependence of the response on the Bi concentration. The highest response was obtained for the Bi concentration of 20%. On the basis of this result, all the nanorod samples for the sensing tests in this study were prepared so that they might have the optimal Bi concentration of 20%.

On the other hand, the responses of the pristine In_2O_3 and Bi_2O_3 nanoparticle-decorated In_2O_3 nanorod sensors to 200 ppm of ethanol gas were examined at different temperatures as shown in Figure 6b to determine the optimal operation temperature. The Bi_2O_3 nanoparticle-decorated In_2O_3 nanorod sensor showed the strongest response at 200 °C, suggesting

DOI: 10.1021/acsami.5b00972
ACS Appl. Mater. Interfaces 2015, 7, 8138−8146

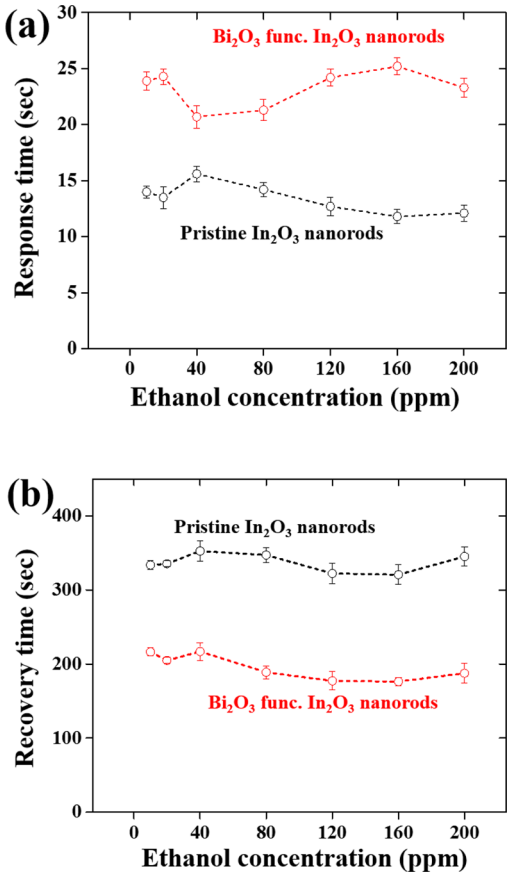

Figure 5. (a) Response times and (b) recovery times of the pristine and Bi_2O_3 nanoparticle-decorated In_2O_3 nanorod gas sensors as a function of the ethanol concentration.

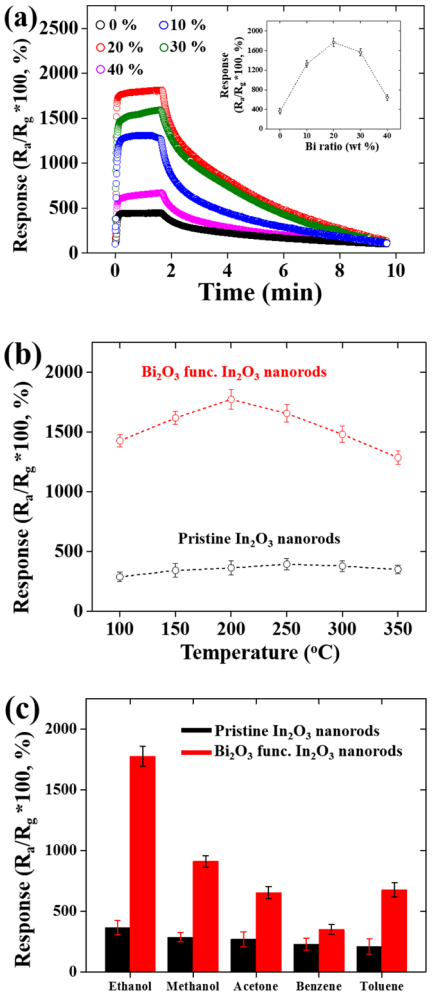

Figure 6. (a) Responses of Bi_2O_3 nanoparticle-decorated In_2O_3 nanorod gas sensors with different Bi concentrations to 200 ppm of ethanol. (b) Responses of pristine and Bi_2O_3 nanoparticle-decorated In_2O_3 nanorod gas sensors to 200 ppm of ethanol as a function the operation temperature. (c) Responses of pristine and Bi_2O_3 nanoparticle-decorated In_2O_3 nanorod gas sensors to different gases at 200 ppm ethanol at 200 °C.

that the optimal operation temperature for the decorated In_2O_3 nanorod sensor is 200 °C, whereas the pristine In_2O_3 nanorod sensor showed almost the same response in the temperature range of 100 to 350 °C. On the basis of these results, all other sensing tests were carried out at 200 °C. At low temperatures, upon exposure to oxygen, because of the inactive ionosorption of oxygen due to rare active adsorption sites at the In_2O_3 and Bi_2O_3 surfaces, inactive oxidation of ethanol gas occurs, resulting in poor response. As the operating temperature increases, the ionosorption of oxygen on the sensor surface becomes active, and oxidation of ethanol becomes more active, resulting in enhanced response to ethanol gas. However, further increases in temperature than the optimal temperature will result in an increase in charge-carrier concentration. The increase in charge-carrier concentration, in turn, will lead to a decrease in Debye length and thereby poor response again. Furthermore, at temperatures higher than the optimal temperature, desorption of all kinds of species will occur.

Figure 6c presents the selectivity of the pristine and Bi_2O_3 nanoparticle-decorated In_2O_3 nanorod sensors to ethanol over other volatile organic compound (VOC) gases: methanol, acetone, benzene, and toluene. The two sensors showed the strongest response to ethanol among different gases with the same concentration (200 ppm) at 200 °C. Why the response of the In_2O_3 nanorods to ethanol at 200 °C is higher than those to other gases is not fully understood at the present. One possible reason is that In_2O_3 possesses electrocatalytic properties of enhancing ethanol oxidation. The ethanol oxidation reaction will be enhanced by In_2O_3, resulting in a more significant increase in electron concentration and a more significant decrease in resistance in the In_2O_3 nanorod sensor than other material sensors. Another reason might be related to the different optimal operating temperatures of the sensor for different target gases. The response of a sensor material to a certain gas might depend on many factors, such as solid solubility of the gas in the material, the decomposition rate of the adsorbed molecule at the material surface, the charge carrier concentration in the material, the Debye length in the material, the catalytic activity of the material,[45,46] the orbital energy of the gas molecule,[47−49] etc. The oxidation rate of a gas is determined by these factors. Therefore, each gas has the characteristic optimal oxidation temperature at which its oxidation rate is maximized. The Bi_2O_3-decorated In_2O_3 nanorod sensor fabricated in this study showed higher response fortunately to ethanol than other gases at 200 °C because of the higher oxidation rate of ethanol at the surface of In_2O_3 and Bi_2O_3 at the temperature, but it might show higher responses to other VOC gases than ethanol at different temperatures.

3.3. Sensing Mechanism of the Bi_2O_3 Nanoparticle-Decorated In_2O_3 Nanorod Gas Sensors. Nanorod-type

DOI: 10.1021/acsami.5b00972
ACS Appl. Mater. Interfaces 2015, 7, 8138−8146

sensors are basically superior to thin film-type sensors in sensitivity and response rate. The smaller radius of the nanorod sensor compared to Debye length of the nanorod material can lead to the complete depletion or accumulation of charge carriers in the nanorod, resulting in a further increase in response to target gas along with the significant increase in the response of the sensor as a result of the high surface-to-volume ratio of the nanorod. Moreover, upon exposure to the target gas, a tunable conducting channel forming at the center of the nanorod along the nanorod axis will be in close contact with the gas as shown in Figure 7a, leading to a short response time.[50]

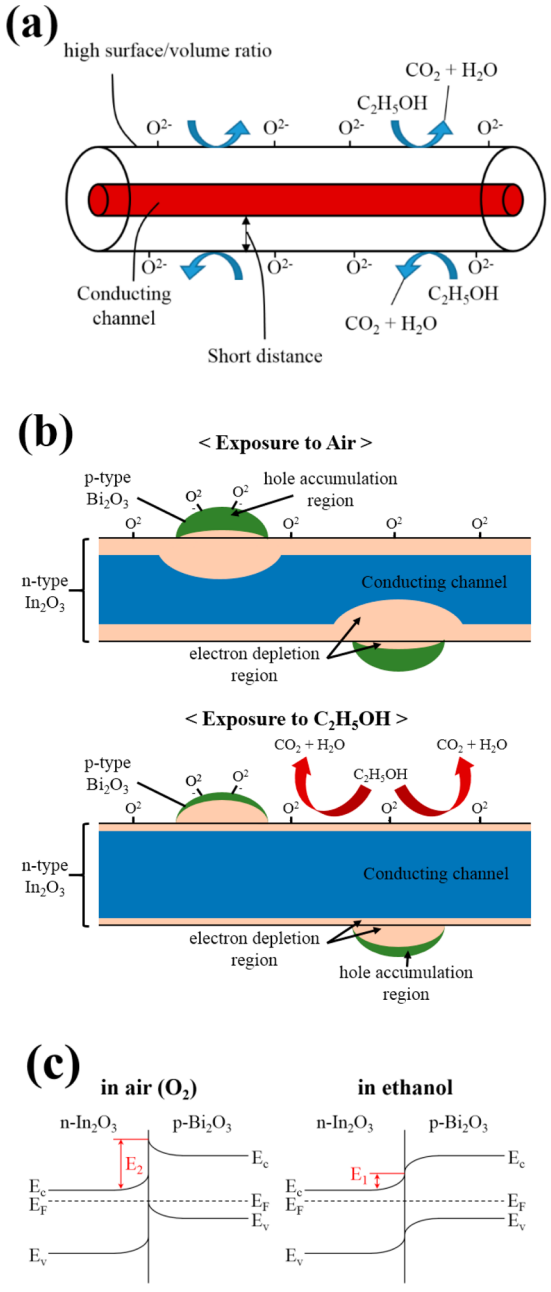

Figure 7. (a) Schematic diagram showing the small radius, as well as the high surface-to-volume ratio of an 1D nanostructure. (b) Schematic diagrams showing the depletion layer and potential barrier forming at the In_2O_3-Bi_2O_3 junction upon exposure to air and C_2H_5OH gas. (c) Energy band diagrams of the In_2O_3-Bi_2O_3 system in air and C_2H_5OH gas.

The sensing mechanism of MOS nanoparticle-decorated semiconductor gas sensors is not well established compared to that of noble metal catalyst-doped or decorated semiconductor gas sensors. The sensing mechanism of MOS nanoparticle-decorated MOS sensors might be closer to that of MOS-core/MOS-shell nanostructured sensors rather than that of metal catalyst-decorated MOS sensors. In MOS nanoparticle-decorated MOS sensors, modulation of the potential barrier height at the interface of a nanoparticle and the matrix of the sensor and the depletion layer width forming at the interface during adsorption and desorption of target gas. On the other hand, in metal catalyst-decorated MOS sensors the catalytic activity or spillover effect of the metal catalyst plays a main role. We may say that the sensing mechanism of the Bi_2O_3-decorated In_2O_3 nanorod sensor fabricated in this study is closer to that of MOS-core/MOS-shell nanostructured sensors because modulation of interface potential energy barrier and interface depletion layer width is predominant over the catalytic activity or spillover effect of the nanoparticle material as discussed below.

In the case of the pristine In_2O_3 nanorod gas sensor, upon exposure to air, the In_2O_3 nanorod surfaces readily adsorb the oxygen molecules in the atmosphere and ionize them to O_2^-, O^-, or O^{2-} by capturing free electrons from the conduction band of In_2O_3, which cause a decrease in carrier concentration and an increase in resistance

$$1/2O_2(g) + e^- = O^-(ad) \quad (1)$$

Upon exposure to ethanol gas, the ethanol gas molecules adsorbed by the In_2O_3 nanorod surface react with the adsorbed oxygen molecules[51]

$$C_2H_5OH + O^{2-} \rightarrow CH_3CHO + H_2O + 2e^- \quad (2)$$

$$CH_3CHO + 5O^{2-} \rightarrow 2CO_2 + 2H_2O + 10e^- \quad (3)$$

Reactions 2 and 3 release electrons to the In_2O_3 nanorod surface, resulting in an increase in electron concentration and a decrease in resistance.

On the other hand, in the Bi_2O_3-decorated In_2O_3 nanorod sensor, different reactions occur on the In_2O_3 surface and Bi_2O_3 nanoparticle surface. When the Bi_2O_3-decorated In_2O_3 nanorod sensor is in air, reaction 1 occur in the surface region of the In_2O_3 nanorod as those in the pristine In_2O_3 nanorod sensor, even though the depletion region somewhat expands in the In_2O_3 nanorod surface because of the formation of the p−n junction between n-type In_2O_3 and p-type Bi_2O_3. When the Bi_2O_3-decorated In_2O_3 nanorod sensor is exposed to ethanol, the depletion region in the surface region of the In_2O_3 nanorod shrinks because of the generation of electrons as a result of reactions 2 and 3.

In contrast, on the p-type Bi_2O_3 nanoparticle surface, upon exposure to air an accumulation layer forms in the Bi_2O_3 nanoparticle as a result of the following reaction as shown in Figure 6b

$$1/2O_2(g) = O^-(ad) + h^+ \quad (4)$$

When the Bi_2O_3 nanoparticle surface is exposed to ethanol, the width of the accumulation layer near the surface is decreased by the following reaction between C_2H_5OH and $O^-(ad)$, making an effect of increasing resistance

$$C_2H_5OH + O^{2-} + 2h^+ \rightarrow CH_3CHO + H_2O \quad (5)$$

DOI: 10.1021/acsami.5b00972
ACS Appl. Mater. Interfaces 2015, 7, 8138−8146

$$CH_3CHO + 5O^{2-} + 10h^+ \rightarrow 2CO_2 + 2H_2O \quad (6)$$

In other words, P-type Bi_2O_3 nanoparticles themselves always behave in an opposite way to n-type In_2O_3 nanorods, which must be a negative effect on the sensitivity of the nanorod sensor. However, the negative effect of the Bi_2O_3 nanoparticles expanding the depletion layer on the In_2O_3 side upon exposure to air is less significant than the positive effect because of the smaller accumulation region due to the smaller size of Bi_2O_3 nanoparticles compared to that of the In_2O_3 nanorods (Figure 7b). That is the reason why the Bi_2O_3-decorated In_2O_3 nanorod sensor showed n-type sensing characteristics. In other words, modulation of the depletion layer width occurs in the sensor accompanying the adsorption and desorption of ethanol gas, which results in the increased resistance change and thereby enhanced sensitivity. The depletion layer forming on the In_2O_3 side in air is known to be expanded in the Bi_2O_3-decorated In_2O_3 nanorod sensor because of the existence of the accumulation on the Bi_2O_3 side,[52] which is one of the positive effects.

Other positive effects of the Bi_2O_3-decorated In_2O_3 nanorod sensor might include modulation of the interface potential barrier height, the high catalytic activity of Bi_2O_3 for the oxidation of ethanol, and creation of more active adsorption sites by Bi_2O_3 nanoparticles. First, one of the important differences between the pristine and Bi_2O_3-decorated In_2O_3 nanorod sensor is the existence of p-n heterojunctions in the latter. A potential barrier develops at the p-Bi_2O_3/n-In_2O_3 interface due to built-in potential (Figure 7c).[52,53] Modulation of the potential barrier height also occurs during the adsorption and desorption of ethanol gas, which might be an additional positive effect on the sensing properties. The potential barrier height at the p−n junction changes from E_1 (in ethanol gas) to E_2 (in air) as shown in Figure 6c. Second, the high catalytic property of Bi_2O_3 on the oxidation of organic species has been reported previously by many groups. Lou et al. reported that the catalytic performance of CO oxidation was significantly enhanced by using Bi_2O_3-decorated Co_3O_4 catalysts.[54] They explained that incorporation of Bi_2O_3 molecules into the lattice of Co_3O_4 caused the structural defect and lattice distortion, which should be the origin of the high O_2 activation ability and mobility. Lu et al. also reported enhanced aerobic oxidation of primary aliphatic alcohols over Bi_2O_3-supported platinum catalysts in water.[55] Precipitation of Bi_2O_3 nanoparticles on the In_2O_3 nanorods creates crystallographic defects at the Bi_2O_3−In_2O_3 interface because of the lattice mismatch between the two materials, which provides preferential adsorption site for ethanol and oxygen molecules.[56] The sensing performance of the Bi_2O_3-decorated In_2O_3 nanorod sensor is believed to be enhanced by the combination of these positive effects.

4. CONCLUSIONS

Unique 1D nanostructures of In_2O_3 decorated with Bi_2O_3 nanoparticles have been synthesized first using a simple one-step process successfully, the preparation process of which is less costly, more environment-friendly and gives less chance for contamination with impurities. The response, sensing speed, and selectivity of the In_2O_3 nanorods for ethanol gas over other gases have been significantly improved by decorating the nanorods with Bi_2O_3 nanoparticles. The optimal Bi concentration in the Bi_2O_3 nanoparticle-decorated In_2O_3 nanorods was found to be 200 °C. The operation temperature has been lowered by decorating nanorods with Bi_2O_3 nanoparticles. Selectivity for ethanol gas has been enhanced by decorating nanorods with Bi_2O_3 nanoparticles.

The underlying mechanism for the enhanced sensing performance of the multiple-networked Bi_2O_3-decorated In_2O_3 nanorod sensor to ethanol gas can be explained by modulation of the depletion layer width forming near the In_2O_3−Bi_2O_3 interface region, modulation of the potential barrier at the In_2O_3−Bi_2O_3 interface, highly catalytic activity of Bi_2O_3 for ethanol oxidation, and the creation of active adsorption sites by Bi_2O_3 nanoparticles. We believe that these results will make a meaningful contribution to the development of an ethanol gas sensor with high performance by showing significantly enhanced ethanol sensing performance of multiple-networked Bi_2O_3-decorated In_2O_3 nanorods.

■ ASSOCIATED CONTENT

Supporting Information

Table S1 showing the raw data of the responses of the pristine and Bi_2O_3 nanoparticle-decorated In_2O_3 nanorod gas sensors as a function of the ethanol concentration, Table S2 showing the raw data of the responses of the pristine and Bi_2O_3 nanoparticle-decorated In_2O_3 nanorod gas sensors as a function of the operation temperature, and Table S3 showing the raw data of the responses of pristine and Bi_2O_3 nanoparticle-decorated In_2O_3 nanorod gas sensors to different gases at 200 ppm ethanol at 200 °C. This material is available free of charge via the Internet at http://pubs.acs.org.

■ AUTHOR INFORMATION

Corresponding Author

*Tel.: +82 32 860 7536. Fax: +82 32 862 5546. E-mail: cmlee@inha.ac.kr.

Notes

The authors declare no competing financial interest.

■ ACKNOWLEDGMENTS

This study was supported by Basic Science Research Program through the National Research Foundation of Korea (NRF) funded by the Ministry of Education (Grant 2010-0020163).

■ REFERENCES

(1) Comini, E.; Faglia, G.; Sberveglieri, G.; Pan, Z.; Wang, Z. L. Stable and highly sensitive gas sensors based on semiconducting oxide nanobelts. *Appl. Phys. Lett.* **2002**, *81*, 1869−1871.

(2) Kolmakov, A.; Moskovits, M. Chemical sensing and catalysis by one-dimensional metal-oxide nanostructures. *Annu. Rev. Mater. Res.* **2004**, *34*, 151−180.

(3) Huang, M. H.; Mao, S.; Feick, H.; Yan, H.; Wu, Y.; Kind, H.; Weber, E.; Russo, R.; Yang, P. Room-temperature ultraviolet nanowire nanolasers. *Science* **2001**, *292*, 1897−1899.

(4) Shehada, N.; Brönstrup, G.; Funka, K.; Christiansen, S.; Leja, M.; Haick, H. Ultrasensitive Silicon Nanowire for Real-World Gas Sensing: Noninvasive Diagnosis of Cancer from Breath Volatolome. *Nano Lett.* **2014**, DOI: 10.1021/nl504482t.

(5) Peng, G.; Tisch, U.; Haick, H. Detection of nonpolar molecules by means of carrier scattering in random networks of carbon nanotubes. *Nano Lett.* **2009**, *9*, 1362.

(6) Wang, D.; Ma, Z.; Dai, S.; Liu, J.; Nie, Z.; Engelhard, M. H.; Huo, Q.; Wang, C.; Kou, R. Low-temperature synthesis of tunable mesoporous crystalline transition metal oxides and applications as Au catalyst supports. *J. Phys. Chem. C* **2008**, *112*, 13499−13509.

(7) Kim, H.; Jin, C.; Park, S.; Kim, S.; Lee, C. H_2S gas sensing properties of bare and Pd-functionalized CuO nanorods. *Sens. Actuators, B* **2012**, *161*, 594−599.

DOI: 10.1021/acsami.5b00972
ACS Appl. Mater. Interfaces 2015, 7, 8138−8146

(8) Park, S.; An, S.; Ko, H.; Lee, S.; Lee, C. Synthesis, structure, and UV-enhanced gas sensing properties of Au-functionalized ZnS nanowires. *Sens. Actuators, B* **2013**, *188*, 1270−1276.
(9) Park, S.; Lee, S.; Kim, H. W.; Lee, C. Hydrogen sensing properties of multiple networked Nb_2O_5/ZnO core-shell nanorod sensors. *Sens. Actuators, B* **2014**, *202*, 840−845.
(10) Tamaki, J.; Shimanoe, K.; Yamada, Y.; Yamamoto, Y.; Miura, N.; Yamazoe, N. Dilute hydrogen sulfide sensing properties of CuO−SnO_2 thin film prepared by low-pressure evaporation method. *Sens. Actuators, B* **1998**, *49*, 121−125.
(11) Lin, L.; Yang, Y.; Men, L.; Wang, X.; He, D.; Chai, Y.; et al. A highly efficient TiO_2@ZnO n-p-n heterojunction nanorod photocatalyst. *Nanoscale* **2013**, *5*, 588−93.
(12) Jin, C.; Park, S.; Kim, H.; Lee, C. Ultrasensitive multiple networked Ga_2O_3-core/ZnO-shell nanorod gas sensors. *Sens. Actuators, B* **2012**, *161*, 223−228.
(13) Park, S.; An, S.; Mun, Y.; Lee, C. UV-enhanced NO_2 gas sensing properties of SnO_2-core/ZnO-shell nanowire at room temperature. *ACS Appl. Mater. Interfaces* **2013**, *5*, 4285−4292.
(14) Hwang, I. S.; Choi, J. K.; Kim, S. J.; Dong, K. Y.; Kwon, J. H.; Ju, B. K.; Lee, J. H. Enhanced H_2S sensing characteristics of SnO_2 nanowires functionalized with CuO. *Sens. Actuators, B* **2009**, *142*, 105−110.
(15) Zhan, Z.; Lu, J.; Song, W.; Jiang, D.; Xu, J. Highly selective ethanol In_2O_3-based gas sensor. *Mater. Res. Bull.* **2007**, *42*, 228−235.
(16) Na, C. W.; Woo, H. S.; Lee, J. H. Design of highly sensitive volatile organic compound sensors by controlling NiO loading on ZnO nanowire networks. *RSC Adv.* **2012**, *2*, 414−417.
(17) Kim, H. J.; Jeong, H. M.; Kim, T. H.; Chung, J. H.; Kang, Y. C.; Lee, J. H. Enhanced ethanol sensing characteristics of In_2O_3-decorated NiO hollow nanostructures via modulation of hole accumulation layers. *ACS Appl. Mater. Interface* **2012**, *6*, 18197−18204.
(18) Kuang, Q.; Lao, C. S.; Liu, Y. Z.; Xie, Z. X.; Zheng, L. S.; Wang, Z. L. Enhanced the photon- and gas-sensing properties of a single SnO_2 nanowire based nanodevice by nanoparticle surface functionalization. *J. Phys. Chem. C* **2008**, *112*, 11539−11544.
(19) Aluri, G. S.; Motayed, A.; Davydov, A. V.; Oleshiko, V. P.; Bertness, K. A.; Sanford, N. A.; Rao, M. V. Highly sensitive GaN-nanowire/TiO_2-nanocluster hybrid sensors for detection of benzene and related environment pollutants. *Nanotechnology* **2011**, *22*, No. 295503.
(20) Choi, S. W.; Katoch, A.; Kim, J. H.; Kim, S. S. Prominent reducing gas-sensing performances of n-SnO_2 nanowires by local creation of p−n heterojunctions by functionalization with p-Cr_2O_3 nanoparticles. *ACS Appl. Mater. Interfaces* **2014**, *6*, 17723−17729.
(21) Na, C. W.; Woo, H. S.; Kim, I. D.; Lee, J. H. Selective detection of NO_2 and C_2H_5OH using a Co_3O_4-decorated ZnO nanowire network sensor. *Chem. Commun.* **2011**, *47*, 5148−5150.
(22) Jin, W.; Dong, B.; Chen, W.; Zhao, C.; Mai, L.; Dai, Y. Synthesis and gas sensing properties of Fe_2O_3 nanoparticles activated V_2O_5 nanotubes. *Sens. Actuators, B* **2010**, *145*, 211−215.
(23) Ling, B.; Sun, X. W.; Shen, Y. Q.; Dong, Z. L. Hierarchical ZnO/Bi_2O_3 nanostructures: synthesis, characterization, and electron-beam modification. *Appl. Phys. A: Mater. Sci. Process.* **2010**, *98*, 91−96.
(24) Li, D.; Zhang, Y.; Zhang, Y.; Zhou, X.; Guo, S. Fabrication of bidirectionally doped β-Bi_2O_3/TiO_2-NTs with enhanced photocatalysis under visible light irradiation. *J. Hazard. Mater.* **2013**, *258*−*259*, 42−49.
(25) Chung, W. Y.; Sakai, G.; Shimanoe, K.; Miura, N.; Lee, D. D.; Yamazoe, N. Preparation of indium oxide thin film by spin-coating method and its gas-sensing properties. *Sens. Actuat. B: Chem.* **1998**, *46*, 139−145.
(26) Liess, M. Electric-field-induced migration of chemisorbed gas molecules on a sensitive film-a new chemical sensor. *Thin Solid Films* **2002**, *410*, 183−187.
(27) Tamaki, J.; Naruo, C.; Yamamoto, Y.; Matsuoka, M. Sensing properties to dilute chlorine gas of indium oxide based thin film sensors prepared by electron beam evaporation. *Sens. Actuators, B* **2002**, *83*, 190−194.
(28) Kiriakids, G.; Bender, M.; Katsarakis, N.; Gagaoudakis, E.; Hourdakis, E.; Douloufakis, E.; Cimalla, V. Ozone sensing properties of polycrystalline indium oxide films at room temperature. *Phys. Status Solidi A* **2001**, *185*, 27−32.
(29) Zheng, W.; Lu, X.; Wang, W.; Li, Z.; Zhang, H.; Wang, Y.; Wang, Z.; Wang, C. A highly sensitive and fast-responding sensor based on electrospun In_2O_3 nanofibers. *Sens. Actuators, B* **2009**, *142*, 61−65.
(30) Elouali, S.; Bloor, L. G.; Binios, R.; Parkin, I. P.; Carmalt, C. J.; Darr, J. A. Gas sensing with nano-indium oxides (In_2O_3) prepared via continuous hydrothermal flow synthesis. *Langmuir* **2012**, *28*, 1879−1885.
(31) Xu, J.; Chen, Y.; Shen, J. Ethanol sensor based on hexagonal indium oxide nanorods prepared by solvothermal methods. *Mater. Lett.* **2008**, *62*, 1363−1365.
(32) Arafat, M. M.; Dinan, B.; Akbar, S. A.; Haseeb, A. S. M. A. Gas sensors based on one dimensional nanostructured metal-oxides: A review. *Sensors* **2012**, *12*, 7207−7258.
(33) Zheng, W.; Lu, X.; Wang, W.; Li, Z.; Zhang, H.; Wang, Z.; Xu, X.; Li, S.; Wang, C. Assembly of Pt nanoparticles on electrospun In_2O_3 nanofibers for H2S detection. *J. Colloid Interface Sci.* **2009**, *338*, 366−370.
(34) Singh, N.; Gupta, R. K.; Lee, P. S. Gold-nanoparticle-functionalized In_2O_3 nanowires as CO gas sensors with a significant enhancement in response. *Appl. Mater. Inter.* **2011**, *3*, 2246−2252.
(35) Kim, S. S.; Park, J. Y.; Choi, S. W.; Kim, H. S.; Na, H. G.; Yang, J. C.; Kim, H. W. Significant enhancement of the sensing characteristics of In_2O_3 nanowires by functionalization with Pt nanoparticles. *Nanotechnology* **2010**, *21*, 415502.
(36) Lin, F. G.; Takao, Y.; Shimizu, Y.; Egashira, M. Zinc oxide varistor gas sensor: effect of Bi_2O_3 content on the H_2-sensing properties. *J. Am. Ceram. Soc.* **1995**, *78*, 2301−2306.
(37) Tomchenko, A. A. Structure and gas-sensitive properties of WO_3-Bi_2O_3 mixed thick films. *Sens. Actuators, B* **2000**, *68*, 48−52.
(38) Kana, S. M.; El-kadri, O. M.; Abu-Yousef, I. A.; Kanan, M. C. Semiconducting metal oxide based sensors for selective gas pollutant detection. *Sensors* **2009**, *9*, 8158−8196.
(39) Montenegro, A.; Ponce, M.; Castro, M. S.; Rodriguez-Paez, J. E. SnO_2-Bi_2O_3 and SnO_2-Sb_2O_3 gas sensors obtained by soft chemical method. *J. Eur. Ceram. Soc.* **2007**, *27*, 4143−4146.
(40) Park, S.; An, S.; Ko, H.; Jin, C.; Lee, C. Enhanced gas sensing properties of Bi_2O_3-core/In_2O_3-shell nanorod gas sensors. *Bull. Korean Chem. Soc.* **2012**, *33*, 3368−3372.
(41) Gou, X.; Li, R.; Wang, G.; Chen, Z.; Wexier, D. Room-temperature solution synthesis of Bi_2O_3 nanowires for gas sensing application. *Nanotechnology* **2009**, *20*, 495501.
(42) Kwon, Y.; Kim, H.; Lee, S.; Chin, I.-J.; Seong, T.-Y.; Lee, W. I.; Lee, C. Enhanced ethanol sensing properties of TiO_2 nanotube sensors. *Sens. Actuators, B* **2012**, *173*, 441−446.
(43) Xu, X.; Fan, H.; Liu, Y.; Wang, L.; Zhang, T. Au-loaded In_2O_3 nanofibers-based ethanol micro gas sensor with low power consumption. *Sens. Actuators, B* **2011**, *160*, 713−719.
(44) Gu, H.; Wang, Z.; Hu, Y. Hydrogen gas sensors based on semiconductor oxide nanostructures. *Sensors* **2012**, *12*, 5517−5550.
(45) Parrondo, J.; Santhanam, R.; Mijangos, F.; Rambabu, B. Electrocatalytic performance of In_2O_3-supported Pt/C nanoparticles for ethanol electro-oxidation in direct ethanol fuel cells. *Int. J. Electrochem. Sci.* **2010**, *5*, 1342−1354.
(46) Choi, K. I.; Kim, H. R.; Kim, K. M.; Liu, D.; Cao, G.; Lee, J. H. C_2H_5OH sensing characteristics of various Co_3O_4 nanostructures prepared by solvothermal reaction. *Sens. Actuators, B* **2010**, *146*, 183−189.
(47) Li, Y.; Xu, J.; Chao, J.; Chen, D.; Ouyang, S.; Ye, J.; Shen, G. High-aspect-ratio single-crystalline porous In_2O_3 nanobelts with enhanced gas sensing properties. *J. Mater. Chem.* **2011**, *21*, 12852−12857.
(48) Wen, Z.; Tianmo, L. Gas-sensing properties of SnO_2-TiO_2-based sensor for volatile organic compound gas and its sensing mechanism. *Phys. B* **2010**, *405*, 1345−1348.

DOI: 10.1021/acsami.5b00972
ACS Appl. Mater. Interfaces 2015, 7, 8138−8146

(49) Feng, C.; Li, W.; Li, C.; Zhu, L.; Zhang, H.; Zhang, Y.; Ruan, S.; Chen, W.; Yu, L. Highly efficient rapid ethanol sensing based on $In_{2-x}Ni_xO_3$ nanofibers. *Sens. Actuators, B* **2012**, *166−167*, 83−88.
(50) Vizcaíno, J. L. P.; Núñez, C. G. Fast, effective manipulation of nanowires for electronic devices. *SPIE Newsroom* **2013**, DOI: 10.1117/2.1201312.005260.
(51) Ivanovskaya, M.; Kotsikau, D.; Faglia, G.; Nelli, P. Influence of chemical composition and structural factors of Fe_2O_3/In_2O_3 sensors on their selectivity and sensitivity to ethanol. *Sens. Actuators, B* **2003**, *96*, 498−503.
(52) Miller, D. R.; Akbar, S. A.; Morris, P. A. Nanoscale metal oxide-based heterojunctions for gas sensing: A review. *Sens. Actuators, B* **2014**, *204*, 250−272.
(53) Park, S.; Ko, H.; Kim, S.; Lee, C. Role of the interfaces in multiple networked one-dimensional core−shell nanostructured gas sensors. *ACS Appl. Mater. Interfaces* **2014**, *6*, 9595−9600.
(54) Lou, Y.; Wang, L.; Zhao, Z.; Zhang, Y.; Zhang, Z.; Lu, G.; Guo, Y. Low-temperature CO oxidation over Co_3O_4-based catalysts: Significant promoting effect of Bi_2O_3 on Co_3O_4 catalyst. *Appl. Catal., B* **2014**, *146*, 43−49.
(55) Lu, T.; Du, Z.; Liu, J.; Ma, H.; Xu, J. Aerobic oxidation of primary aliphatic alcohols over bismuth oxides supported platinum catalysts in water. *Green Chem.* **2013**, *15*, 2215−2221.
(56) Zhang, H.; Feng, J.; Fei, T.; Liu, S.; Zhang, T. SnO_2 nanoparticles-reduced graphene oxide nanocomposites for NO_2 sensing at low operating temperature. *Sens. Actuators, B* **2014**, *190*, 472−478.

DOI: 10.1021/acsami.5b00972
ACS Appl. Mater. Interfaces 2015, 7, 8138−8146